ChemComm

COMMUNICATION

View Article Online
View Journal | View Issue

Cite this: *Chem. Commun.*, 2023, 59, 12471

Received 6th May 2023,
Accepted 25th September 2023

DOI: 10.1039/d3cc02212a

rsc.li/chemcomm

A ferrocene-modified stable metal–organic framework for efficient CO_2 photoreduction reaction†

Gui-Qi Lai,‡[a] Ning Li,‡[a] Jun He *[a] and Ya-Qian Lan *[b]

A series of ferrocene-grafted/loaded stable metal–organic frameworks (MOFs), based on the classical NH_2-MIL-125(Ti), were prepared to improve the light absorption and photogenerated charge migration of photocatalysts, which can achieve enhanced CO_2-to-HCOOH reduction performance. This work highlights the obvious advantage of the modifiability of the MOF structure in optimizing the performance of the photocatalytic CO_2RR.

Metal–organic frameworks (MOFs), as a class of well-defined and tunable crystalline porous materials, have shown great advantages in the field of CO_2 photoreduction.[1–5] For instance, high product selectivity and activity can be achieved through the establishment of specific catalytic active sites in MOFs.[6–13] However, considering the importance of catalyst photosensitivity, rapid photogenerated charge migration, and structural stability to improve the performance of the CO_2 photoreduction reaction (CO_2RR), it remains difficult to find suitable MOF photocatalysts that can satisfy these structural features simultaneously.[14–16] Although the addition of noble metal photosensitizers to the reaction system can improve the light absorption capacity of the MOF, it also increases the reaction cost.[17] Therefore, the best solution is to achieve the above structural properties in the same MOF catalyst.

We believe that a strategy can be adopted to realize the above idea by grafting photosensitized and electron-conducting functionalized groups on the stable MOF structure using a post-synthesis approach. In this case, the stable MOF can be modified by functionalized groups not only to increase the photosensitivity but also to achieve fast photogenerated charge transport.[9,18–22] Ferrocene (Fc) has been shown to be a good electron donor and has the ability to transfer electrons rapidly.[23–25] Moreover, ferrocene-modified crystalline complexes also often exhibit excellent light absorption ability through ligand–metal interactions resulting in strong charge transfer effects.[26–28] Therefore, it may be a good candidate to verify our idea if the ferrocenes are grafted on the stable MOF structure.

Based on the above considerations, we chose the classical **NH_2-MIL-125(Ti)** (denoted as **NM**) as a stable MOF catalyst carrier and constructed a series of Fc-grafted (by post-synthetic aldehyde amine condensation) or ferrocene-loaded (by pore encapsulation) MOF catalysts, namely **Fca-NH_2-MIL-125(Ti)-(1–2)** (denoted as **FNM-1–2**, where $N_{NH2}:N_{Fca}$ are 1 : 1 and 1 : 10) and **Fc@NH_2-MIL-125(Ti)** (denoted as **F@NM**), respectively (Fig. 1). The introduction of Fc groups by post-synthesis significantly enhanced the light absorption and charge transfer ability of the MOF catalysts. The photocatalytic results show that all MOF materials could complete the photocatalytic CO_2RR in water and exhibited progressively higher photocatalytic activity. Among them, the photocatalytic performance of **FNM-2** was the best among these MOF materials; its photocatalytic activities under UV and visible light irradiation were 293.40 and 266.33 μmol g^{-1} h^{-1}, and the selectivities of formic acid products were both close to 100%. This work highlights the obvious advantage of the modifiability of the

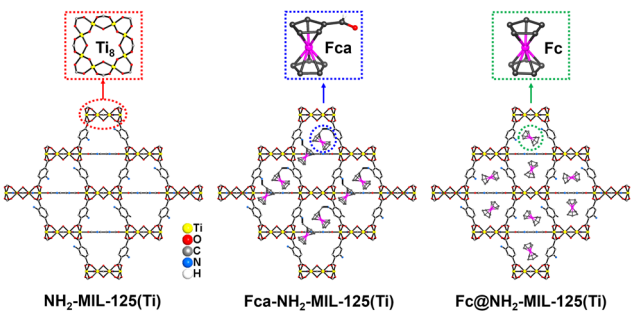

Fig. 1 Schematic view of the structures of **NM**, **FNM-1–2** and **F@NM**.

[a] *School of Chemical Engineering and Light Industry, Guangdong University of Technology, Guangzhou 510006, Guangdong, China. E-mail: junhe@gdut.edu.cn*
[b] *School of Chemistry, South China Normal University, Guangzhou 510006, PR China. E-mail: yqlan@m.scnu.edu.cn*

† Electronic supplementary information (ESI) available: Experimental details and general procedures; and XRD, FTIR, and gas adsorption data. See DOI: https://doi.org/10.1039/d3cc02212a

‡ These authors contributed equally to this work.

MOF structure in improving the performance of the photocatalytic CO_2RR.

The **NM** was prepared according to the reported synthetic method. Fc grou-grafted MOF materials (**FNM-1–2**) were synthesized by considering the reaction of amino groups (in **NM**) with ferrocenecarbaldehyde (Fca) in different material dosage feeding ratios. The Fc group-loaded MOF material (**F@NM**) was prepared by immersing the **NM** crystals and stirring in a saturated ferrocene methanol solution. The experimentally synthesized **FNM-1–2** and **F@NM** were washed several times by DMF and methanol solvents to remove the adhering Fca/Fc molecules from the crystal surface and the free Fca molecules inside the pores, followed by drying at 80 °C for 12 h in a vacuum oven.

Powder X-ray diffraction (PXRD) characterization confirmed that Fc-grafted/loaded MOF materials maintained the pristine **NM** structure (Fig. 2a).[6] Scanning electron microscopy (SEM) also showed that the crystal morphologies of **FNM-1–2** and **F@NM** were almost identical to the parent **NM** ellipsoidal morphology, with sizes in the range of 0.5–1 μm (Fig. 3a–d). From the thermogravimetric analysis (TGA) curves of **NM**, it can be found that Fc-grafted/loaded MOFs (**FNM-1–2** and **F@NM**) have different weight losses to the parent **NM** (Fig. S1, ESI†). The solid UV-vis absorption spectra showed that **NM** containing $-NH_2$ chromophores possesses obvious visible light absorption ability (close to 500 nm), and the colors of the MOF materials after grafting and loading ferrocene substrates were deepened and the light absorption range was further extended close to 800 nm (Fig. 2b). Based on the Tauc curves, the calculated band gaps (E_g) of **FNM-1–2** and **F@NM** were 1.92, 1.82 and 1.99 eV, exhibiting distinct semiconductor-like properties (as shown in Fig. 2c). Ultraviolet photoelectron spectroscopy (UPS) was further used to determine the HOMO–LUMO energy level distributions of **NM**, **FNM-1–2**, and **F@NM** with their corresponding LUMO energy levels of −1.85, −1.62, −1.0, and −0.79 V (*vs.* NHE). Considering the negative LUMO levels of these MOF materials, they are potential photocatalysts for the CO_2RR thermodynamically (as shown in Fig. 2d and Fig. S2, ESI†). To accurately calculate the content of the grafted or loaded functional ferrocenes, an inductively coupled plasma emission spectrometer (ICP) was further employed to determine the content of Fe and Ti in these MOF materials. The results showed that the mass ratios of Fe and Ti were 1 : 4.3 (**FNM-1**), 1 : 1.8 (**FNM-2**) and 2.1 : 1 (**F@NM**). Therefore, the actual successful grafting ratios of the ferrocenes for one Ti_8 cluster with six $-NH_2$ groups were calculated to be $N_{NH2} : N_{Fe}$ = 3.2 : 1, 1.4 : 1 in **FNM-1–2**. However, the actual successful loading ratio ($N_{NH2} : N_{Fe}$) of ferrocene in **F@NM** obtained by physical agitation was 1 : 2.8. This result indicates that the loading capacity of ferrocene was much larger than the grafting amount. In addition, we further tested the N_2 and CO_2 adsorption properties of the MOF materials containing ferrocenes (Fig. S3–S6, ESI†). Obviously, the BET, pore size distribution, and CO_2 adsorption of the MOF materials modified with different contents of functionalized ferrocene substrates showed a regular decrease compared to the prototype **NM** (1386.63 $m^2\ g^{-1}$), which again proved that the ferrocene substrates were successfully grafted or loaded into the MOF.

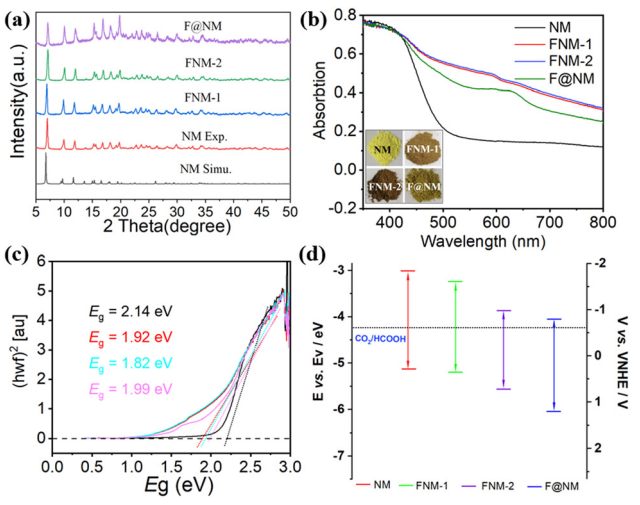

Fig. 2 (a) PXRD of **NM**, **FNM-1–2** and **F@NM**. (b) Solid state UV-vis absorption of **NM**, **FNM-1–2** and **F@NM**. (c) $(hwf)^2$ *vs.* $h\nu$ curves of **NM**, **FNM-1–2** and **F@NM**. (d) The energy band structure diagram for **NM**, **FNM-1–2** and **F@NM**.

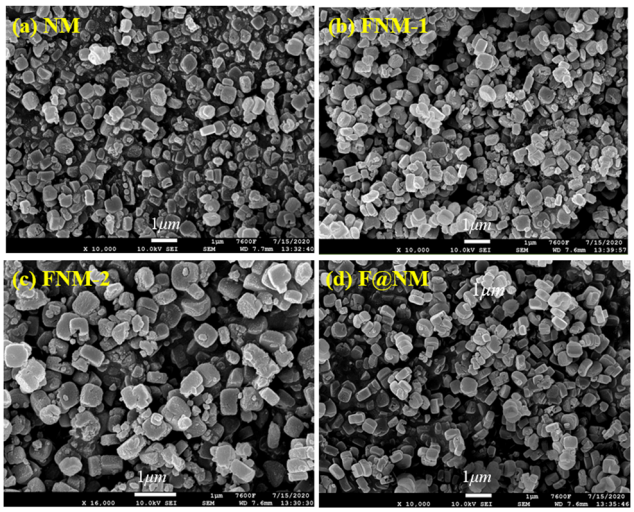

Fig. 3 The SEM images of **NM**, **FNM-1**, **FNM-2** and **F@NM**.

The UV/visible light-irradiated CO_2RR of the activated MOF materials was performed under a pure CO_2 (1.0 atm, 293 K) atmosphere in pure H_2O with triethanolamine (TEOA) as an electron sacrificial agent donor, without any photosensitizer or precious metal cocatalyst. As shown in Fig. 4a, under visible light irradiation, HCOOH was the only reduction product detected by ion chromatography (IC) with yields of 67.33 (**NM**), 136.33 (**FNM-1**), 266.33 (**FNM-2**), and 88.66 μmol $g^{-1}\ h^{-1}$ (**F@NM**). No gas phase reduction products were observed in gas chromatography (GC), demonstrating that the product HCOOH selectivity was close to 100%. When UV light (200–400 nm) was used to excite the photocatalytic CO_2RR (Fig. 4b), the reduction products included not only the liquid-phase product HCOOH but also a small amount of the gas-phase

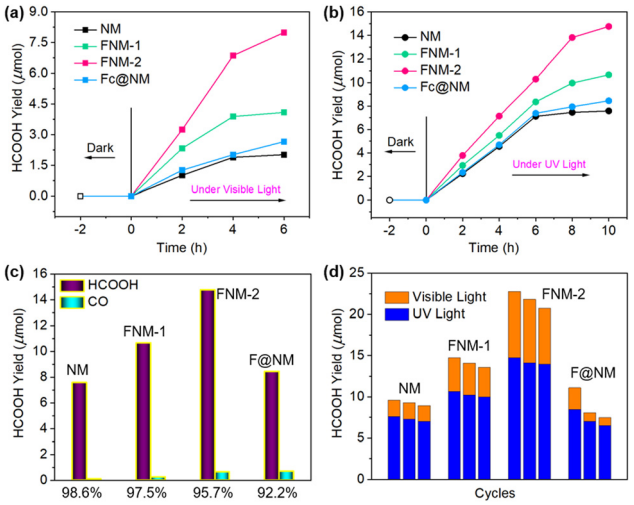

Fig. 4 (a) and (b) The amount of HCOOH produced as a function of the time of UV and visible light irradiation over **NM**, **FNM-1**, **FNM-2** and **F@NM**. (c) and (d) The product selectivity and catalytic durability of **NM**, **FNM-1**, **FNM-2** and **F@NM**.

product CO. The yields of HCOOH for **NM**, **FNM-1–2** and **F@NM** were 151.60, 213.20, 293.40 and 169.0 μmol g^{-1} h^{-1}, respectively, corresponding to the HCOOH selectivity of 98.6%, 97.5%, 95.7%, and 92.2% (Fig. 4c). Obviously, the photocatalytic performance of **FNM-1–2** was higher than that of the parent **NM** and **F@NM** under both visible and UV light irradiation. Moreover, the photocatalytic performance showed an increasing trend with the increase of the amount of grafted ferrocene. The UV light-excited photocatalytic performance is slightly higher than that of the visible light, which may be attributed to the weak visible light absorption ability of these MOF materials. However, the visible light absorption ability of **FNM-1–2** and **F@NM** was significantly enhanced compared to the parent **NM**, which increased the utilization of sunlight by the MOFs and thus improved the final photocatalytic performance. The stability and long-term CO_2RR experiment of these MOF catalysts was evaluated by cycling reactions (Fig. 4d). It was found that the photocatalysts maintained almost their initial activity with good catalytic sustainability after three cycles. However, there was an unavoidable mass loss in the photocatalyst recycling process, resulting in a slight decrease in the amount of HCOOH produced. The most significant decrease in catalyst mass after the cycling reaction is **F@NM**, which may be attributed to the partial leaching of the loaded ferrocenes from the MOF. The transient photocurrent response values of these MOFs under visible light irradiation were **F@NM** > **FNM-2** > **FNM-1** > **NM** (Fig. S7, ESI†). Obviously, ferrocene-loaded **F@NM** exhibited the strongest photogenerated charge transfer ability, but its photocatalytic activity was lower than that of the ferrocene-grafted **FNM-1–2**. We speculate that the **F@NM** excites photogenerated charge transfer to the photocatalytic active site mainly through close spatial distances and π–π stacking with organic ligands, while the ferrocene substrates grafted by chemical bonding may have more efficient photogenerated charge transfer efficiency. This fact suggests that the ferrocene substrates can effectively increase the photogenerated charge transfer rate of MOFs, thus contributing to the improved photocatalytic performance.

After the reaction, the MOF material photocatalysts were removed from the reaction solution, and the leaching rates of Fe^{2+} and Ti^{4+} ions in the catalytic filtrate by inductively coupled plasma (ICP) analysis were 0.0012%, 0.0017% and 0.00042% (Fe); 0.0021%, 0.0038%, 0.002% and 0.098% (Ti). The UV-vis absorption spectrum of the post-reaction filtrate showed no significant absorption signal other than the solvent peak (Fig. S8, ESI†). Importantly, no significant changes were observed in the IR, PXRD and XPS spectra before and after the CO_2RR (Fig. S9–S14, ESI†). To demonstrate the photocatalytic activity of these MOF materials, we performed a series of control experiments lacking light, CO_2, TEOA, or MOF material catalysts (Table S1, ESI†). Regardless of the lack of any of these conditions, the photocatalytic CO_2RR could not proceed, and neither ion chromatography nor gas chromatography detected any photocatalytic reduction products. Moreover, these ferrocene-based MOFs are among the superior photocatalysts for CO_2-to-HCOOH conversion (Table S2, ESI†).

To verify the origin of the products, isotopic $^{13}CO_2$ ($^{13}CO_2$ atmosphere) tracking experiments were performed under the same CO_2RR conditions with **FNM-2** as a representative photocatalyst, and the resulting carbon-based reduction products were characterized by ^{13}C NMR spectroscopy. As shown in Fig. S15 (ESI†), the $HCOO^-$ signal at 163.9 ppm was clearly observed, which is consistent with the previous work.[10,29–32] These experimental results clearly demonstrate that the carbon source in the $HCOO^-$ produced by the photocatalytic CO_2RR is indeed from the reaction atmosphere CO_2, and further indicates their photocatalytic CO_2 to HCOOH reduction activity.

It has been previously reported that **NM** can complete the photocatalytic reduction of CO_2 to HCOOH and their reaction mechanism has been demonstrated by isotope tracking experiments and characterized by EPR experiments.[6,23,31] In this work, *in situ* electron paramagnetic resonance (EPR) characterization was performed to investigate the role of ferrocene. As shown in Fig. S16 (ESI†), **NM**, **FNM-2** and **F@NM** did not show EPR signals in the dark under a N_2 atmosphere. When imposing light under the same reaction conditions, an obvious Ti^{3+} species signal (g = 1.941) appeared in **NM** (Fig. S16a, ESI†), while ferrocene-based MOFs (**FNM-2** and **F@NM**) produced both Ti^{3+} and high-spin Fe^{3+} (g = 4.281) signals (Fig. S16b and c, ESI†). Moreover, the intensity of Ti^{3+} and Fe^{3+} species was further enhanced with the increase of the light duration. This phenomenon is mainly attributed to the fact that Ti^{4+} in the Ti-oxo core of these MOFs receives photogenerated electrons *via* ligand-to-cluster charge transfer and is then reduced to Ti^{3+} species. In contrast, ferrocene, which is known as a good electron donor, can also generate and transfer electrons under photoexcitation and thus be oxidized to Fe^{3+} species itself. When the reaction system continued to be illuminated by light and passed into a CO_2 atmosphere, Ti^{3+} and Fe^{3+} signals were significantly weakened and finally disappeared. This fact

indicated that Ti^{3+} and Fe^{3+} species were involved in the photocatalytic CO_2 reduction reaction. Based on the EPR characterization results, the photocatalytic reaction mechanism of these MOF materials can be rationalized as follows: (i) **NM**, **FNM-1**, **FNM-2** and **F@NM** can absorb light and excite electron–hole pairs by grafted or loaded ferrocene groups and $-NH_2$ co-chromophores simultaneously under light irradiation. Among them, the ferrocene moiety can be used for effective electron storage and donor, which effectively improves the efficiency of the catalyst itself for photogenerated charge transfer. Subsequently, through the effective charge transfer interaction, the photogenerated electrons stemmed from ferrocenes and $-NH_2$ chromophores are subsequently separated and transferred to the Ti_8 metal-oxo core, while the generated photogenerated holes remain on the ferrocene or organic ligand; (ii) the Ti^{4+} ions in the Ti_8 metal-oxo core accept the transferred photogenerated electrons to be reduced to Ti^{3+} ions, and the TEOA in the reaction system is used as an electron sacrificial donor to quench the photo-generated holes left on the ferrocene (Fe^{3+} back to Fe^{2+}) or the organic ligand; (iii) the Ti^{3+} ions then provide the photo-excited electrons for the activation of the CO_2 molecules adsorbed, and lose electrons themselves to return to the Ti^{4+} ion state again. In this way, these MOF catalysts complete the CO_2 to HCOOH photosynthesis reaction cycle mainly by using the metal intervalence conversion (Ti^{3+}–Ti^{4+} and Fe^{2+}–Fe^{3+}) in the structure. In addition, the titanium-oxo cluster itself can absorb UV light and be excited to generate photogenerated electron–hole pairs. The photogenerated electrons are transferred to Ti ions *via* O^{2-} for activation of CO_2 molecules, while the holes are quenched by the TEOA sacrificial agent in the reaction system.

In summary, the functionalized ferrocenes are loaded in the stable **NM** structure by chemical bond grafting or pore-limiting effect. The functional group-modified stable MOF materials can exhibit a wider UV-vis absorption range and stronger charge transfer effects than the parent structures. Based on these advantages, they can exhibit higher photocatalytic CO_2RR performance compared to the parent MOF. This work also demonstrates that functionalized modification of crystalline MOF materials can provide more possibilities for solving specific structural needs of catalysts.

This work was financially supported by the National Natural Science Foundation of China (No. 22201046, 21871061, and 21871141), the China Postdoctoral Science Foundation (2021M700877 and No. 15 Special Fund (In-Station), 2022T150143) and the Local Innovative and Research Teams Project of Guangdong Pearl River Talents Program (2017BT01Z032).

Conflicts of interest

There are no conflicts to declare.

References

1 Y. Chen, D. K. Wang, X. Y. Deng and Z. H. Li, *Catal. Sci. Technol.*, 2017, **7**, 4893–4904.
2 C. S. Diercks, Y. Liu, K. E. Cordova and O. M. Yaghi, *Nat. Mater.*, 2018, **17**, 301–307.
3 R. Li, W. Zhang and K. Zhou, *Adv. Mater.*, 2018, **30**, e1705512.
4 C. Wang, Z. Xie, K. E. deKrafft and W. Lin, *J. Am. Chem. Soc.*, 2011, **133**, 13445–13454.
5 Y. Liu, Y. Yang, Q. Sun, Z. Wang, B. Huang, Y. Dai, X. Qin and X. Zhang, *ACS Appl. Mater. Interfaces*, 2013, **5**, 7654–7658.
6 Y. Fu, D. Sun, Y. Chen, R. Huang, Z. Ding, X. Fu and Z. Li, *Angew. Chem., Int. Ed.*, 2012, **51**, 3364–3367.
7 S. Wang, W. Yao, J. Lin, Z. Ding and X. Wang, *Angew. Chem., Int. Ed.*, 2014, **53**, 1034–1038.
8 Y. Lee, S. Kim, J. K. Kang and S. M. Cohen, *Chem. Commun.*, 2015, **51**, 5735–5738.
9 D. Sun, W. Liu, M. Qiu, Y. Zhang and Z. Li, *Chem. Commun.*, 2015, **51**, 2056–2059.
10 H.-Q. Xu, J. Hu, D. Wang, Z. Li, Q. Zhang, Y. Luo, S.-H. Yu and H.-L. Jiang, *J. Am. Chem. Soc.*, 2015, **137**, 13440–13443.
11 D. Chen, H. Xing, C. Wang and Z. Su, *J. Mater. Chem. A.*, 2016, **4**, 2657–2662.
12 H. Zhang, J. Wei, J. Dong, G. Liu, L. Shi, P. An, G. Zhao, J. Kong, X. Wang, X. Meng, J. Zhang and J. Ye, *Angew. Chem., Int. Ed.*, 2016, **55**, 14310–14314.
13 Y. Wang, N. Y. Huang, J. Q. Shen, P. Q. Liao, X. M. Chen and J. P. Zhang, *J. Am. Chem. Soc.*, 2018, **140**, 38–41.
14 X. Chang, T. Wang and J. Gong, *Energy Environ. Sci.*, 2016, **9**, 2177–2196.
15 X. Liu, S. Inagaki and J. Gong, *Angew. Chem., Int. Ed.*, 2016, **55**, 14924–14950.
16 T. Zhang and W. Lin, *Chem. Soc. Rev.*, 2014, **43**, 5982–5993.
17 Y.-H. Luo, L.-Z. Dong, J. Liu, S.-L. Li and Y.-Q. Lan, *Coord. Chem. Rev.*, 2019, **390**, 86–126.
18 D. Sun, Y. Fu, W. Liu, L. Ye, D. Wang, L. Yang, X. Fu and Z. Li, *Chem. – Eur. J.*, 2013, **19**, 14279–14285.
19 L. Li, S. Zhang, L. Xu, J. Wang, L.-X. Shi, Z.-N. Chen, M. Hong and J. Luo, *Chem. Sci.*, 2014, **5**, 3808–3813.
20 D. Sun, W. Liu, Y. Fu, Z. Fang, F. Sun, X. Fu, Y. Zhang and Z. Li, *Chem. – Eur. J.*, 2014, **20**, 4780–4788.
21 T. Luo, J. Zhang, W. Li, Z. He, X. Sun, J. Shi, D. Shao, B. Zhang, X. Tan and B. Han, *ACS. Appl. Mater. Interfaces*, 2017, **9**, 41594–41598.
22 Z.-H. Yan, M.-H. Du, J. Liu, S. Jin, C. Wang, G.-L. Zhuang, X.-J. Kong, L.-S. Long and L.-S. Zheng, *Nat. Commun.*, 2018, **9**, 3353.
23 J. J. Liu, N. Li, J. W. Sun, J. Liu, L. Z. Dong, S. J. Yao, L. Zhang, Z. F. Xin, J. W. Shi, J. X. Wang, S. L. Li and Y. Q. Lan, *ACS Catal.*, 2021, **11**, 4510–4519.
24 Q. Niu, Q. Huang, T.-Y. Yu, J. Liu, J.-W. Shi, L.-Z. Dong, S.-L. Li and Y.-Q. Lan, *J. Am. Chem. Soc.*, 2022, **144**, 18586–18594.
25 J.-L. Hou, W. Luo, Y. Guo, P. Zhang, S. Yang, Q.-Y. Zhu and J. Dai, *Inorg. Chem.*, 2017, **56**, 6451–6458.
26 J.-J. Liu, S.-N. Sun, J. Liu, Y. Kuang, J.-W. Shi, L.-Z. Dong, N. Li, J.-N. Lu, J.-M. Lin, S.-L. Li and Y.-Q. Lan, *J. Am. Chem. Soc.*, 2023, **145**, 6112–6122.
27 Y. Fan, H.-M. Li, R.-H. Duan, H.-T. Lu, J.-T. Cao, G.-D. Zou and Q.-S. Jing, *Inorg. Chem.*, 2017, **56**, 12775–12782.
28 C. Wang, N. Chen, S. Wang and F. Kong, *Inorg. Chem. Front.*, 2022, **9**, 5616–5623.
29 M. Elcheikh Mahmoud, H. Audi, A. Assoud, T. H. Ghaddar and M. Hmadeh, *J. Am. Chem. Soc.*, 2019, **141**, 7115–7121.
30 N. Li, J. Liu, J. J. Liu, L. Z. Dong, Z. F. Xin, Y. L. Teng and Y. Q. Lan, *Angew. Chem., Int. Ed.*, 2019, **58**, 5226–5231.
31 N. Li, J. Liu, J. J. Liu, L. Z. Dong, S. L. Li, B. X. Dong, Y. H. Kan and Y. Q. Lan, *Angew. Chem., Int. Ed.*, 2019, **58**, 17260–17264.
32 N. Li, J.-J. Liu, J.-W. Sun, B.-X. Dong, L.-Z. Dong, S.-J. Yao, Z. Xin, S.-L. Li and Y.-Q. Lan, *Green Chem.*, 2020, **22**, 5325–5332.

